Math Geosci (2020) 52:355–379
https://doi.org/10.1007/s11004-019-09816-6

SPECIAL ISSUE

Optimization of a SAG Mill Energy System: Integrating Rock Hardness, Solar Irradiation, Climate Change, and Demand-Side Management

Julian M. Ortiz[1] · **Willy Kracht**[2,3] · **Giovanni Pamparana**[2,3] · **Jannik Haas**[4,5]

Received: 15 December 2018 / Accepted: 6 June 2019 / Published online: 1 July 2019

Abstract Integration of renewable energy into mining and processing operations is becoming necessary as part of a strategy towards sustainability in the minerals industry. A solar photovoltaic plant along with a battery energy storage system (PV-BESS) can provide a long-term solution to cope with increasing energy costs, thus reducing the tension with other societal competing needs for a key resource such as clean energy. However, sizing these systems is challenging, in face of uncertain ore grindability and solar power availability. In this paper, we present an application of an integrated model to size the PV-BESS, where the variability of ore grindability is modeled using geostatistical tools, solar irradiance variability is captured using a Markov chain simulation model, and the entire system is optimized through linear stochastic optimization, considering a fixed mine schedule for the feed of a semiautogenous grinding (SAG) mill. The main goals are to minimize the costs associated with operating the SAG mill in the presence of a PV-BESS system, understand how the sizing and costs change under the influence of stochastic drivers, and reveal the potential for demand-side management in mines. The size and costs of the necessary infrastructure are determined for a model of estimated grindability and an ensemble of 50 simulated models of grindability, and compared against the sizing and cost of the ground truth. The effect of climate change on solar energy availability is accounted for by forecasting the ratio of excellent, good,

✉ Julian M. Ortiz
julian.ortiz@queensu.ca

1 Robert M. Buchan Department of Mining, Queen's University, Kingston, Canada

2 Department of Mining Engineering, Universidad de Chile, Santiago, Chile

3 Advanced Mining Technology Center (AMTC), Universidad de Chile, Santiago, Chile

4 Energy Center, Universidad de Chile, Santiago, Chile

5 Department of Stochastic Simulation and Safety Research (IWS/RC SimTech), University of Stuttgart, Stuttgart, Germany

and moderate days over bad days in terms of irradiance out to the year 2030. Finally, the effects of stockpiles and feed control according to the processing plant needs, namely a demand-side management approach, are evaluated to reveal the impact on the energy requirements and the sizing of the photovoltaic and storage system. The model is optimized considering a yearly cost function, with hourly resolution for the solar irradiance and hardness models. The results show that integrating solar power into the operation of a SAG mill has potential to reduce the total energy cost by 27%. Robustness against climate change can be achieved with an increase in total cost of 1%. Finally, use of stockpiles to manage the ore supply to the mill and minimize the energy cost to process it results in a cost reduction of around 2%, which should offset the rehandling cost of managing the stockpiles.

Keywords Geometallurgy · Geostatistics · Cosimulation · Solar energy

1 Introduction

Sustainable mining extraction requires revisiting the approach mining companies take in relation to consumption of key resources for society, such as water and energy (ICMM 2014; Levesque et al. 2014; Moran and Kunz 2014). Grinding, and comminution in general, are known to be responsible for a significant proportion of the total energy consumption in mining. Some accounts indicate that comminution consumes up to 4% of global electrical energy and accounts for about 50% of the total energy consumed by a mining operation (Wei and Craig 2009; CEEC 2013; Bouchard et al. 2017). Reductions in energy consumption can undoubtedly be achieved through process control (Bouchard et al. 2017) or optimizing grinding media (de Bakker 2014), but this should be combined with integration of renewable energies (Giurco et al. 2014).

Solar power is one such alternative source of energy that can be used in conjunction with fuel-based sources to supply the requirements of mining operations and processing plants. Some attempts have been made to incorporate solar energy into operating mines (Paraszczak and Fytas 2012; Choi and Song 2017). The potential use of solar energy also becomes more attractive in remote operations as the capital and operating costs of these technologies decrease (Haas et al. 2017). A significant amount of work has been done to characterize the solar energy resource available in different parts of the world, particularly in places with high solar potential (Zweibel et al. 2007; Clifton and Boruff 2010; Ortega et al. 2010; Ministerio de Energía de Chile 2018) to provide information for potential users, such as the mining industry.

In mining, there are many challenges for the integration of solar energy into the supply for processes and operations. One of these challenges is the need to commit to a size for the solar plant and storage system. In this paper, the focus is on the sizing of a photovoltaic plant and battery energy storage system (PV-BESS) to provide energy to a specific process, namely the operation of a semiautogenous grinding (SAG) mill. Of course, this decision carries risks related to the availability of solar energy, which depends on the irradiance potential at the location where the PV plant is installed, combined with the energy requirement of the SAG mill, which depends on the ore fed into the process. The ore will have variable grindability, which can be characterized

on site by testing representative volumes of rock. These samples can be used to build a spatial model of the grindability in a resources block model. The resources are mined out in a specific sequence defined by the mine plan, thus converting the three-dimensional distribution of grindability into a one-dimensional time series.

To add complexity to this problem, climate change is causing a clear variation in the solar availability in some places of the world (Schaeffer et al. 2012). This adds another dimension to the analysis of a long-term decision such as the construction of a PV-BESS.

It has been previously shown that the optimum size of the PV-BESS facility depends on the fluctuations of the grindability of the rock fed into the processing plant, combined with the variable hourly patterns of irradiance for the generation of solar energy (Pamparana et al. 2019a, b). This suggests the use of a different approach to reduce the cost of energy consumption and make best use of the PV-BESS infrastructure by changing the feed to synchronize the grindability to the instantaneous cost of energy, that is, processing soft rock that requires less energy per ton when the energy cost is high, but hard rock that requires more energy per ton when the energy is low. The concept of demand-side management (DSM) has been used successfully in some mine operations (Pelzer et al. 2008; Matthews and Craig 2013), offering the possibility of a paradigm change in terms of adjusting the mine plan to optimize an objective function that integrates the revenues associated with the metal content recovered in combination with the energy costs associated with their processing. Furthermore, this demand-side management strategy may also strongly impact the need for energy storage systems. So far, scientific literature lacks a systematic assessment regarding the PV-BESS design in combination with demand-side management strategies under the impact of climate change. This is the goal of the present work.

The general methodology is presented first, outlining the steps required to build the different models involved in the final sizing decision. The results of an optimization for a synthetic study are then presented for cases where forecasts are done without and with accounting for climate change. Conclusions and an outlook of the potential of this technology are provided at the end.

2 Methodology

The goal of this work is to assess the size of a photovoltaic (PV) system and battery energy storage system (BESS), along with the energy contract with the grid, to minimize the total energy cost incurred from operating a SAG mill. The capital expenditure associated with the PV-BESS system is prorated over the lifespan of the battery system. This is done accounting for the variability of the grindability of the ore entering the SAG mill, and the variability of the solar energy that characterizes the location of the PV plant. The analysis is expanded to consider the case where stockpiles are used to manage the grindability of the SAG mill feed, and also by assessing potential changes in the solar energy available based on a forecast of the solar availability out to 2030.

Figure 1 shows the energy sources involved in the optimization problem. The photovoltaic (PV) system provides energy during daylight hours. The amount of energy

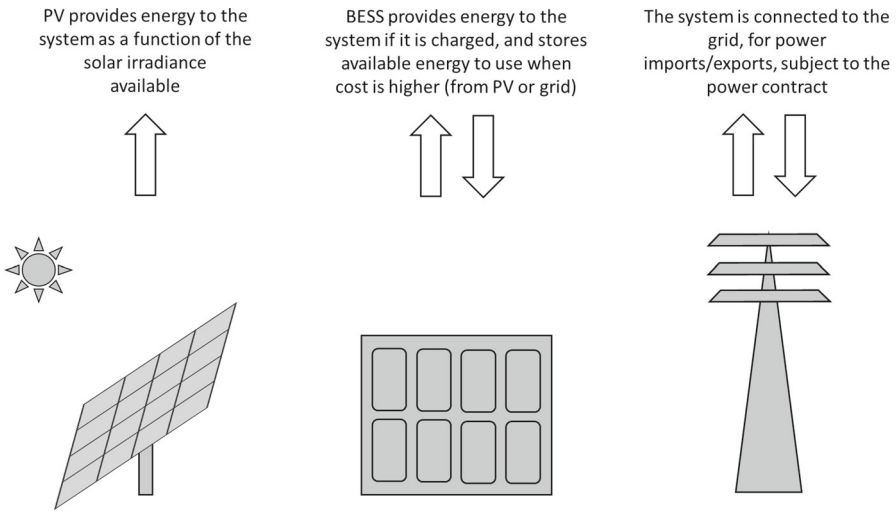

Fig. 1 Energy sources involved in the optimization

depends on the solar irradiance, which varies depending on the meteorological conditions. The battery energy storage system (BESS) can store energy from the PV cells or from the grid, in order to provide energy when PV power is not available at night, or when the grid cost is higher during the day because the grid contract has been exceeded. Finally, the grid provides energy at a contracted cost up to a limit, and charges a penalty if the demand is higher than that contracted limit. It can also buy energy from the PV system or from the BESS.

An optimization is carried out to minimize the yearly cost of energy for the operation of the SAG mill. This cost includes the energy consumption cost in \$/kWh and the capital cost for the PV-BESS infrastructure, prorated over the life of the battery system, accounting for the discount rate through an annuity factor (Pamparana et al. 2019a, b). The energy requirements are defined by the SAG mill consumption, which in turn depends on the feed. This feed depends on the in situ ore grindability and the specific extraction sequence and any potential homogenization that may occur by using stockpiles. Two key inputs are required to infer the energy balance in time:

- First, the time series of the grindability z_{SPI} of the materials fed into the processing plant. This time series, in turn, is linked to the in situ model of the ore resources, which are extracted following a schedule defined by the short-term mine plan to optimize the grades z_{Cu} fed into the plant (Fig. 2). To add complexity to this problem, consideration is given to the possible use of two stockpiles, one for soft rock and one for hard rock (Fig. 3). Note that the rock grindability is estimated from a limited number of metallurgical tests carried out on samples distributed in space.
- Second, the time series of solar irradiance determines the energy that can be provided by the PV-BESS plant. The energy can be harvested and stored in the battery system, or used directly by the SAG mill. The energy can also be sold back to the grid. The energy in the BESS will likely be fully utilized during

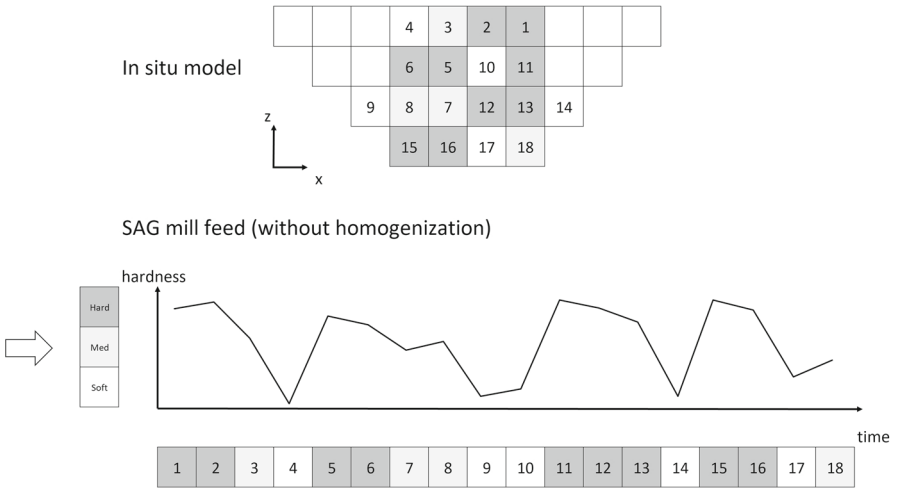

Fig. 2 Conversion of in situ grindability model into time series

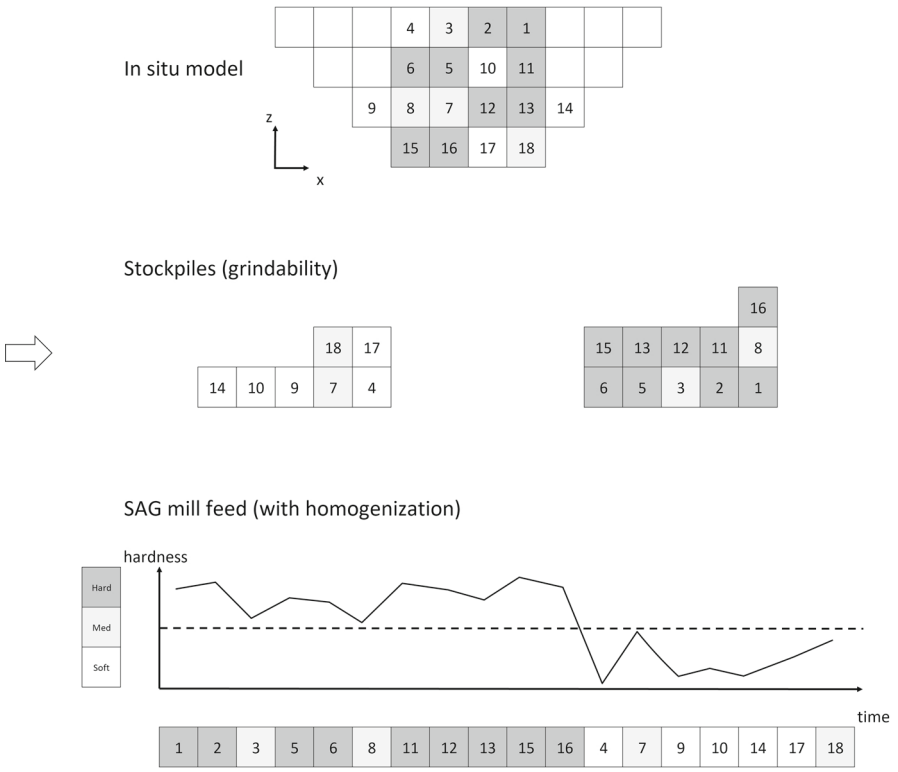

Fig. 3 Conversion of in situ grindability model into time series, considering two stockpiles for homogenization

the night by the SAG mill requirements. One last nuisance for the solar model is that there is a need to forecast solar irradiance, potentially for many decades. Despite the trends in climate change, this factor is rarely considered. In this study, a forecast of the solar irradiance trends is performed to determine the impact that climate change may have over the coming decades for this type of energy source.

Variability plays a key role in the sizing of the PV-BESS installation, since short peaks of high energy demand may be supplied by the grid, at a penalty, and this may be cheaper in the long run than having a larger PV-BESS system. The same happens with the fluctuations in the solar irradiance, which will also impact the size of the PV-BESS system. For example, a sequence of several cloudy days may translate into a high cost to acquire energy from the grid, if the contracted energy is underestimated, incurring a potentially very high penalty.

2.1 Modeling In Situ Rock Hardness Uncertainty

Rock grindability, $z_{\mathrm{SPI}}(u_\alpha)$, can be characterized at location u_α through a relatively conventional test called the SAG power index (SPI) test. This test is performed using a few kilograms of material, coming from rejects of a diamond drillhole sample (Starkey and Dobby 1996). The test can be applied over a set of n samples distributed in space $\{z_{\mathrm{SPI}}(u_\alpha), \alpha = 1, \ldots, n\}$, representative of one of the relevant ore domains $S_k, k = 1, \ldots, K$, which are henceforth called geometallurgical units, in order to build a spatial model of the distribution of grindability $\{Z_{\mathrm{SPI}}(u), u \in S_k\}$. $Z_{\mathrm{SPI}}(u)$ represents a random variable at location u. The model $\{Z_{\mathrm{SPI}}(u), u \in S_k\}$ represents a random function, where the random variables $Z_{\mathrm{SPI}}(u)$ show some spatial correlation.

Conventional geostatistical techniques can be used both to model the distribution of relevant geometallurgical units $\{S(u), u \in D\}$, and estimate or simulate SPI within these domains $\{Z_{\mathrm{SPI}}(u), u \in S_k\}$ for $k = 1, \ldots, K$. Typically, the geometallurgical units are linked to some geological properties of the rock such as lithology, mineralization zone, or alteration (Ortiz et al. 2015; Garrido et al. 2018), and can be modeled by using indicator simulation (Journel and Isaaks 1984), plurigaussian methods (Armstrong et al. 2003), or multiple-point simulation (Perez and Ortiz 2011; Mariethoz and Caers 2014). SPI can then be modeled inside these domains $\{S_k, k = 1, \ldots, K\}$ by means of a Gaussian simulation method for continuous variables (Chiles and Delfiner 2012). Grades are the key driver for the feed to the processing plant. Therefore, the relationship between grades and SPI should be accounted for by means of a joint spatial model $\{(Z_{\mathrm{SPI}}(u), Z_{\mathrm{Cu}}(u)), u \in D\}$.

Geometallurgical variables can be challenging to model when they are nonadditive. This means that the scaling from point samples to block volumes obtained by simply averaging the point estimates, or equivalently, by applying a change of support in the estimation via block kriging, may be biased,

$$\frac{1}{|V|} \int_{u \in V} Z_{\mathrm{SPI}}(u) \mathrm{d}u \neq Z^V_{\mathrm{SPI}}(u), \tag{1}$$

where $Z_{\mathrm{SPI}}(u)$ represents the grindability at sample support and $Z^{V}_{\mathrm{SPI}}(u)$ represents the true grindability at block support. Some solutions to this problem have been proposed, by modeling the change of support using power-law reexpressions (Deutsch 2015). However, to apply this approach, experimental data are required.

For the purposes of this study, a cascade approach is used, where the geometallurgical units $\{S(u), u \in D\}$ are modeled by sequential indicator simulation (Deutsch 2006), and SPI is jointly modeled with copper grade $\{(Z_{\mathrm{SPI}}(u), Z_{\mathrm{Cu}}(u)), u \in D\}$ using sequential Gaussian cosimulation (Manchuk and Deutsch 2012), within the domains defined previously. Multiple realizations are developed to capture the variability associated with the spatial distribution of geometallurgical units and SPI distribution within the units.

2.2 Transferring Rock Hardness to the Processing Plant Feed

The in situ distribution of rock grindability characterized through the SPI must now be transferred to the time series of the SAG mill feed. However, the key driver for the processing plant is the copper production. Copper grade and throughput along with the recovery will determine the concentrate production. Grindability is an operational constraint and is also strongly related to the throughput; therefore it drives the business along with the copper grade to achieve the planned metal production. Thus, a fixed mine plan exists that determines the schedule $\{Z_{\mathrm{Cu}}(u_t), t = 1, \ldots, T\}$, where u_t is the location of the block of ore extracted at time t in the schedule. The selection of blocks sent to the processing plant depends on the copper grade estimated from dense blasthole data $Z^{*}_{\mathrm{Cu}}(u)$. The sequence of grindability in the blocks fed to the plant $\{Z_{\mathrm{SPI}}(u_t), t = 1, \ldots, T\}$ is thus a consequence of this mine sequence.

2.3 Managing Rock Hardness Fed to the Plant: Demand-Side Management

The plant will receive a feed that satisfies the copper grade requirement, but with a high variability of ore grindability (Fig. 2). This is detrimental to the plant performance in terms of its energy requirements. One solution to this problem is to create stockpiles to homogenize and serve as buffers between the discrete operation of trucks and the crusher and the continuous operation of the SAG mill (Fig. 3). For this study, two stocks are considered: one for hard rock and one for soft rock. The first blocks assigned to the stock become the first blocks fed to the plant when demanded. Hard rock is associated with high specific energy consumption, and soft rock, with low specific energy consumption. Keeping the throughput constant, but selecting high or low specific energy consumption blocks for the SAG mill feed allows the energy requirement to be managed, while satisfying the production. Note that this approach does not change the mine plan, but only modifies the daily arrangement of blocks by sending hard material when the energy cost is low and soft material when it is high, in order to achieve the same throughput at lower cost.

Table 1 Definition of day types for solar irradiation model

Type	Daily generation
Excellent (E)	95–100% of maximum daily generation for that month
Good (G)	85–95% of maximum daily generation for that month
Moderate (M)	60–85% of maximum daily generation for that month
Bad (B)	0–60% of maximum daily generation for that month

2.4 Modeling Solar Irradiance Variability

Solar irradiance is measured at some meteorological stations. For the purpose of the study presented here, it is assumed that the PV plant is located in the northern part of Chile, in the Atacama Desert. Information is available through the "Explorador Solar" initiative (Ministerio de Energía de Chile 2018), from which an hourly record is available for the period 2004–2016. From this information, days are classified depending on the maximum daily energy generation capacity (Table 1) for each month. This provides an idea of the solar availability in different months of the year and enables assessment of any climate trend.

The solar irradiance is simulated to account for the variability expected for a given year in the future. This is done by building a Markov chain of day types according to Table 1, where day types are simulated based on transition probabilities built on a monthly basis. This means that all days from a specific month over the available solar data are pooled together to infer the prior probability and the probability of transition from one day type to another.

The prior probabilities of days of type $i \in \{\text{E, G, M, B}\}$ for month m are determined from the historical dataset. The subscript "(0)" refers to the case where probabilities have not been corrected to account for climate change

$$p^m_{i,(0)} = \frac{n^m_{i,(0)}}{\sum_{i\in\{\text{E,G,M,B}\}} n^m_{i,(0)}}, \tag{2}$$

where $n^m_{i,(0)}$ are the frequencies of days of type i for month m. Transition probabilities are calculated for days of the same month in a similar fashion as

$$p^m_{ij,(0)} = \frac{n^m_{ij,(0)}}{\sum_{i\in\{\text{E,G,M,B}\}} \sum_{j\in\{\text{E,G,M,B}\}} n^m_{ij,(0)}}, \tag{3}$$

where $n^m_{ij,(0)}$ are the frequencies of transitions from days of type i to days of type j for month m. Then, from an initial day type, the sequence of day types is simulated using these transition probabilities. The hourly irradiance values for a day simulated in the sequence through the Markov chain are assigned by means of hot deck imputation; that is, the full record of 24-hourly irradiance is pasted from a day of the same type and month, selected randomly from the available data (Izenman 2008).

Several simulated sequences of hourly irradiance can be generated in this fashion and used to account for the expected variability in solar energy generation at the PV plant.

2.5 Forecasting Solar Irradiance: Climate Change

Climate change may have an effect on the available solar power for PV generation (Li et al. 2012; Ohunakin et al. 2015), which could change the optimum decision about the sizing of the PV-BESS infrastructure. To consider this factor, a relatively simple trend analysis is done over the 13 years of available data, and a forecast model is used to modify the transition probabilities for different day types, and hence the marginal probabilities.

The prior probabilities of days in each one of the four proposed classes are computed for each year from the available database. Additive log ratios (alr) are then calculated for each year to account for the fact that the four categories are constrained by the total number of days in the year (Tolosana-Delgado et al. 2018). The additive log ratios for year y computed with respect to bad (B) days are

$$\mathrm{alr}^{y}_{l,(0)} = \ln\left(\frac{p^{y}_{l,(0)}}{p^{y}_{\mathrm{B},(0)}}\right), \tag{4}$$

where $p^{y}_{l,(0)}$ are the prior probabilities of days of type $l \in \{\mathrm{E}, \mathrm{G}, \mathrm{M}\}$ and $p^{y}_{\mathrm{B},(0)}$ is the prior probability for days of type B in year y. For each alr, a linear regression can be performed to forecast the proportion of days in each category in year $y = y_0$

$$\widehat{\mathrm{alr}^{y=y_0}_{l,(0)}} = m_l \cdot y_0 + n_l, \tag{5}$$

where m_l and n_l are the slope and intersect of the regression line corresponding to the alr l.

Monthly transition probabilities are then updated (Eq. 6) to ensure that the global yearly proportions match the forecast. The subscript "(1)" refers to the case where probabilities have been corrected. Transition probabilities in warm months are affected by a fixed set of factors, while transition probabilities in cold months are affected by a different set of factors

$$p^{m}_{ij,(1)} = p^{m}_{ij,(0)} \cdot f^{s}_{ij}, \tag{6}$$

where $p^{m}_{ij,(1)}$ is the updated transition probability from days of type i to days of type j in month m, and f^{s}_{ij} is an updating factor that depends on the cold (May until October, $s = \mathrm{C}$) or warm season (November to April, $s = \mathrm{W}$). f^{s}_{ij} is obtained by calibration to match the frequencies of different day types when the yearly proportions change due to the trends inferred from Eq. 5.

The forecasted alr must be backtransformed to the updated marginal proportions of each day type, by applying closure to the inverse of the log ratios

$$p_{l,(0)}^{y=y_0} = \text{alr}^{-1}\left(\ln\left(\frac{p_{l,(0)}^{y}}{p_{\text{B},(0)}^{y}}\right)\right) = C\Big[\exp\Big(\Big[P_{l,(0)}^{y};0\Big]\Big)\Big]. \tag{7}$$

The correction factors f_{ij}^{s}, $s \in \{\text{C}, \text{W}\}$ are determined such that the marginal probabilities obtained using the corrected transition probability matrices match the forecasted marginal probabilities for each day type, over the year

$$\left\{p_{i,(0)}^{y=y_0}\right\}_{i\in\{\text{E,G,M,B}\}} = \left\{p_{ij,(1)}^{y=y_0}\right\}_{i,j,\in\{\text{E,G,M,B}\}}^{w} \cdot \left\{p_{i,(0)}^{y}\right\}_{i\in\{\text{E,G,M,B}\}}, \tag{8}$$

where $\left\{p_{i,(0)}^{y=y_0}\right\}_{i\in\{\text{E,G,M,B}\}}$ is the vector of updated marginal probabilities of the different day types for the year y_0, $\left\{p_{ij,(1)}^{y=y_0}\right\}_{i,j,\in\{\text{E,G,M,B}\}}$ is the matrix of updated transition probabilities obtained by combining the monthly updated transition probability matrices $p_{ij,(1)}^{m}$, w is a large integer to achieve convergence of the marginal probabilities, and $\left\{p_{i,(0)}^{y}\right\}_{i\in\{\text{E,G,M,B}\}}$ is the initial vector of marginal probabilities of the different day types. In summary, two sets of 16 factors (for cold and warm months) are found so that the aggregated monthly marginal probabilities from the updated monthly transition probability matrices match the target forecasted marginal probabilities from the regression model.

2.6 Optimization Model

The optimization model minimizes an objective function that combines the investment cost of the PV-BESS infrastructure, the contracted energy cost from the grid, and the operational cost of the PV-BESS. All costs are prorated to a yearly basis, accounting for a discount rate, and depend on the life of the batteries, which in turn depends on the number of charge cycles of the storage. Costs are used based on 2020 estimates (Child et al. 2017). The optimization model imposes constraints related to providing sufficient energy to comply with the energy demand of the SAG mill at all times, limits to the charging and discharging capacities of the BESS component to ensure a longer battery life, and costing associated with the contracted energy from the grid and the overconsumption. Similar stochastic optimization models have been used in the context of production scheduling in mining (Goodfellow and Dimitrakopoulos 2017; Lamghari 2017). We now provide a simplified description of the optimization model.

The objective function to minimize is the total yearly cost incurred to satisfy the required energy demand

$$\min f = C^{\text{inv}} + C^{\text{con}} \cdot p^{\text{con}} + E\left(C_y^{\text{op}}\right). \tag{9}$$

This includes:

1. The investment cost C^{inv}, which includes the investment in the PV solar plant and in the BESS system brought to an annual basis using a discount rate. These investments depend on the maximum generating capacity.
2. The contracted power cost from the grid $C^{\text{con}} \cdot p^{\text{con}}$, i.e., the cost per MW multiplied by the contracted power capacity.
3. The expected operational cost over a set of energy requirement scenarios $E\left(C_y^{\text{op}}\right)$, composed of the operational costs related to
   (a) The generator, i.e., maintenance of the solar PV plant
   (b) The storage, i.e., the battery replacement cost on a per-MW basis, which depends on the number of charge/discharge cycles
   (c) The grid, i.e., the costs of importing/exporting energy to the grid
   (d) Operational penalties due to overconsumption from the grid beyond the contracted energy

The optimization is constrained by several conditions:

1. The yearly generated power profile of the PV plant is limited by the PV plant capacity;
2. The BESS power capacity is limited by the charging and discharging capacities of the equipment;
3. The BESS energy balance must be imposed, considering that the BESS capacity also depends on the charging and discharging efficiencies of the batteries;
4. The energy balance of the overall system must include the sum of all the energy inputs and outputs, and must match the SAG mill's energy consumption;
5. The grid contracted energy establishes a maximum amount to be imported, with any overconsumption above the contracted energy from the grid incurring a penalty.

A detailed description of the optimization setup and parameters used can be found in Pamparana et al. (2019a, b).

3 Case Study

3.1 Model Setup

3.1.1 In Situ Model

The simulated model studied is generated respecting the statistical and spatial distributions obtained from real data collected at a porphyry copper deposit to impose realistic statistical and spatial distributions of the geometallurgical domains, the SPI, and copper (Cu) grade over a domain that represents a realistic volume for long-term production (10 years). Model dimensions are presented in Table 2.

SPI and copper grade sample values from three typical geometallurgical units in a porphyry copper deposit are available. The distribution of geometallurgical units is simulated with sequential indicator simulation. SPI and copper grade distributions are jointly modeled with sequential Gaussian cosimulation, accounting for a linear relationship ($\rho = 0.55$). A linear model of coregionalization is fit to the experimental

Table 2 Model dimensions

Coordinate	Number of blocks	Dimensions (m)
East (X)	150	10.0
North (Y)	150	10.0
Elevation (Z)	8	12.0

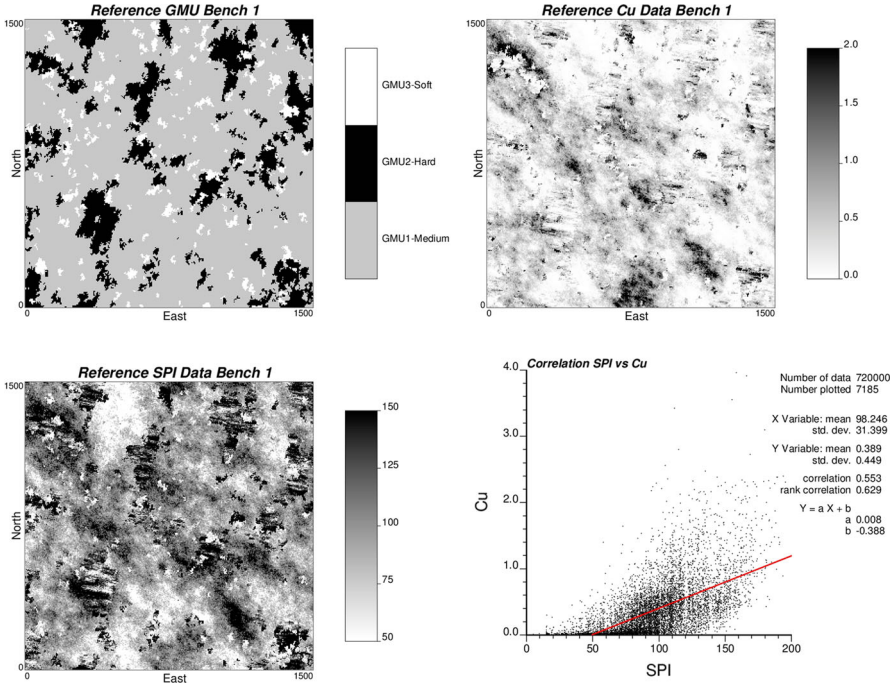

Fig. 4 Reference spatial distributions of geometallurgical units, copper grade, and SPI. The scatter plot between SPI and copper grades is provided (only 1% of the simulated points are shown)

direct and cross variograms (not shown). Maps at point support (every block is represented by four points) and the scatter plot showing the relationship between the SPI and grade are shown in Fig. 4.

This simulated model represents the ground truth (see Fig. 5 for block statistics), and defines the copper grades on which the mine schedule is based. It is used for all subsequent comparisons. A cutoff grade of 0.3% Cu is applied to assign the blocks to the processing plant. This determines the sequence of SPI values to be fed into the SAG mill.

The ground truth is sampled on a 50 m $\times$ 50 m grid to represent a geometallurgical campaign. These samples are used to create an estimated model of SPI with ordinary kriging to account for the fact that, in reality, SPI is not known everywhere in the domain. Copper grades from the ground truth at block support are used to create the mine sequence, since for simplicity, it is assumed that the short-term grade model from blastholes is precise enough to correctly assign each block to the processing plant (which is not true in practice). The estimated SPI model is presented in Fig. 6.

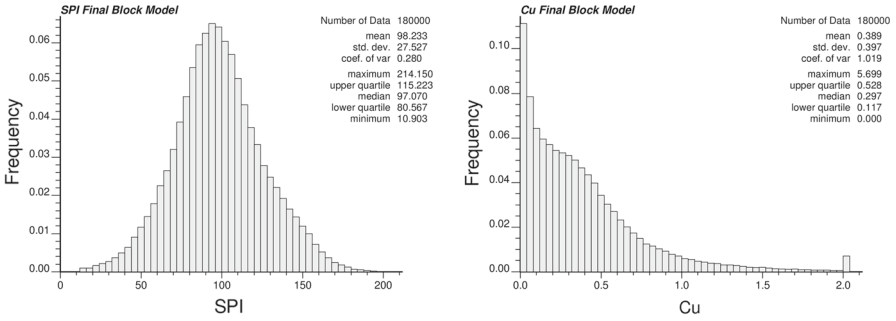

Fig. 5 Histograms and statistics of SPI and copper grade at block support

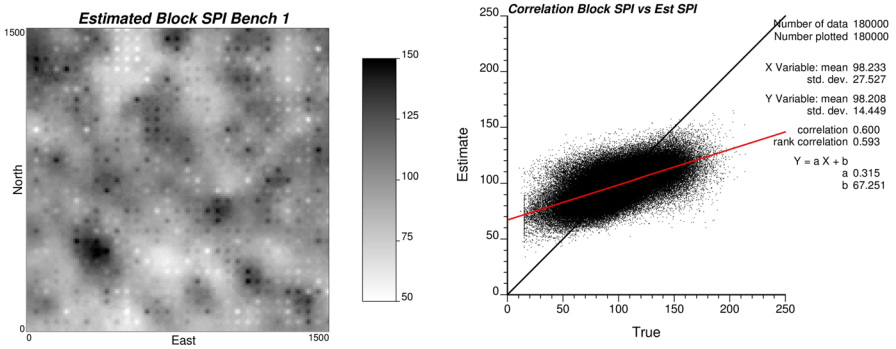

Fig. 6 Estimated SPI and correlation with ground truth

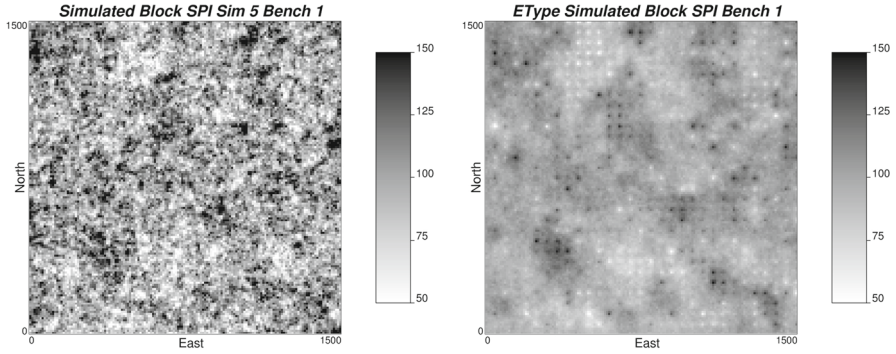

Fig. 7 Simulated SPI and E-type model from 50 realizations

To model the uncertainty associated with SPI, 50 realizations conditional to the sampled SPI values over the 50 m $\times$ 50 m grid are built using sequential Gaussian simulation. Figure 7 shows one simulation at block support and the E-type estimate over 50 realizations (average of the ensemble of conditional simulations), for the same bench displayed in Figs. 4 and 6. It can be seen that the general trends are correctly reproduced, delineating volumes of hard and soft rock.This completes the generation

Table 3 Average and forecasted counts of day types and their corresponding log ratios

Case	Excellent	Good	Moderate	Bad	Total	ln(E/B)	ln(G/B)	ln(M/B)
Average 2004–2016	48.69	208.15	97.00	11.15	365	1.55	3.03	2.26
Forecast 2030	93.03	168.76	75.46	27.75	365	1.21	1.81	1.00

of the in situ spatial models of reserves used for planning. As mentioned above, the mine sequence is applied considering the copper grades from the reference model. This defines the following time series:

1. *Ground truth*: the time series of true block SPI values from the ground truth model.
2. *Estimated*: the time series of estimated block SPI values from the limited samples over the 50 m $\times$ 50 m grid.
3. *Simulated [1–50]*: the time series of simulated block SPI values from the limited samples over the 50 m $\times$ 50 m grid.

3.1.2 Solar Model

The simulated model is located in the Atacama Desert, in northern Chile, where hourly data of solar irradiance are available from the Explorador Solar (Ministerio de Energía de Chile 2018) for the period between 2004 and 2016. Monthly classification thresholds are determined as a function of the maximum daily irradiance within each month over the 13 years. The total count of day types per month and the corresponding additive log ratios (alr) are computed, and presented in the "Appendix." Transition probability matrices are computed for each month. An example is presented in the "Appendix."

Based on the alr for each of the 13 years of information, a linear regression is applied to forecast these log ratios out to 2030 (Fig. 8). All three log ratios decrease in time. The linear decreasing model is conservative, as a cumulative sum analysis (not shown) revealed a dramatic change in the ratios starting in 2014. Based on these linear regressions, the forecasted log ratios and corresponding data type counts for 2030 are presented in Table 3. This trend reflects an increase in the count of bad and excellent days during the year, balanced with a decrease in good and moderate days. Correction factors f_{ij}^{s} are found to update the transition probabilities in the cold and warm months, in order to match the forecasted marginal probabilities obtained from the counts of day types presented in Table 3.

Two models of solar irradiance are considered. The original (current) and updated transition matrices (forecast year 2030) are used to simulate the sequence of day types. The corresponding hourly solar irradiance is simulated by hot deck imputation, where the 24-hourly irradiance of a day of the simulated type in the corresponding month is directly drawn from the available data.

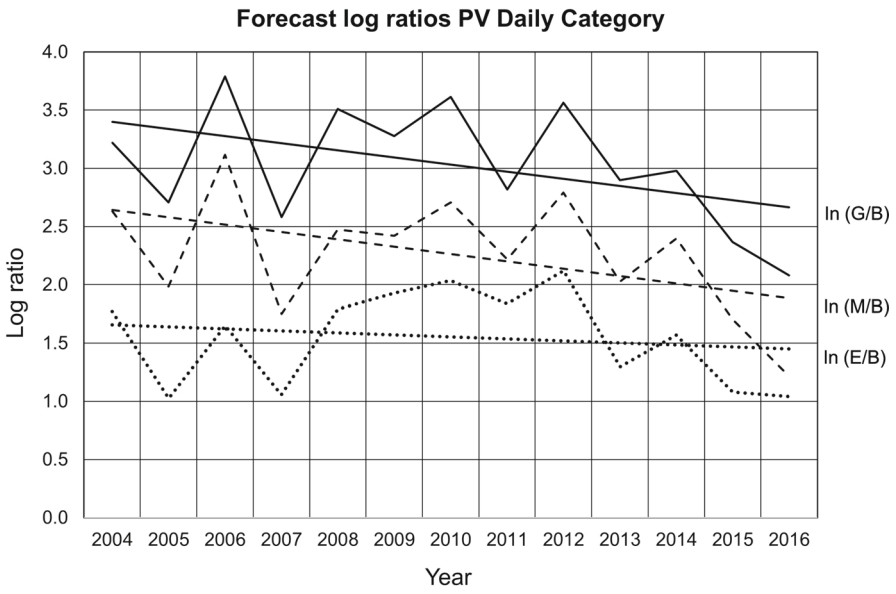

Fig. 8 Log ratio regression models

3.1.3 Demand-Side Management

To complete the experimental settings used in this application, consideration is given to a demand-side management (DSM) approach, where the SAG mill can determine the feed used depending on the cost of the energy and/or some other objective function, such as maximizing the percentage of renewable energy used by the system or minimizing the CO_2 emissions. This is achieved by using two stockpiles of limited capacity, to classify ore as hard or soft, depending on its expected grindability (Fig. 3). The SAG mill will draw from one of the two stockpiles at will to minimize the energy cost. If one of the stocks is emptied, the ore from the other stockpile is used. Stockpiles are modeled using a first-in first-out approach. In our application, a simplified heuristic is used to feed hard rock during the day and soft rock during the night.

3.1.4 Final Cases Studied

The final cases analyzed in the next section are compared by looking at the following outputs of the optimization model:

1. Size of the power contract (MW).
2. Size of the BESS system (MW).
3. Size of the PV plant (MW).
4. Yearly cost (objective function) (USD/year).
5. Operational cost of imports (USD/year).

The cases are summarized in Table 4.

Table 4 Summary of cases analyzed

Case	SPI model	Solar model	PV-BESS	DSM
0 (no PV-BESS)	Ground truth	Current	No	No
1a	Ground truth	Current	Yes	No
2a	Ground truth	Current	Yes	Yes
3a	Ground truth	Forecast 2030	Yes	No
4a	Ground truth	Forecast 2030	Yes	Yes
1b	Estimated	Current	Yes	No
2b	Estimated	Current	Yes	Yes
3b	Estimated	Forecast 2030	Yes	No
4b	Estimated	Forecast 2030	Yes	Yes
1c	Simulated	Current	Yes	No
2c	Simulated	Current	Yes	Yes
3c	Simulated	Forecast 2030	Yes	No
4c	Simulated	Forecast 2030	Yes	Yes

3.2 Results

Results of the optimization are presented in Table 5 for the current solar model and in Table 6 for the forecasted solar model. All values are presented relative to case 1a, that is, the use of a PV-BESS sized using the ground truth, under the current solar conditions and without considering DSM (Figs. 9, 10).

Results in Tables 5 and 6 show the objective function assessed with the input time series of SPI, which is either estimated or simulated.

3.2.1 Results Based on Ground Truth SPI Time Series

The first important result is that not using a PV-BESS (case 0) implies a much higher energy cost for the SAG mill, which translates into a 37% increase in total yearly cost (Table 5, objective function value of case 0), with respect to the case of implementing the PV-BESS (case 1a). The use of a forecasted solar model creates a slight increase in the total cost (case 3a) of about 1%, which may be explained by the increase in excellent and bad days and the compensating change. The use of DSM reduces the cost by about 2% for both solar models. This means that, as long as the cost of rehandling ore to manage the stockpiles does not offset this 2% cost reduction, it is advantageous to consider this option. It should be pointed out that stockpiles were not optimized to minimize the energy cost in this application, but instead fixed sizes were defined, which could be revised to improve the DSM performance.

Finally, the power contract with the grid is 4% larger if PV-BESS is not considered (case 0), and 6% smaller when considering DSM (cases 2a and 4a), with respect to the comparable cases (1a and 3a, respectively).

Table 5 Results for current solar model

Current solar model	0 GT (%)	1a GT (%)	1b EST (%)	1c SIM (%)	2a GT DSM (%)	2b EST DSM (%)	2c SIM DSM (%)
Power contract	104.43	100.00	93.64	92.17	93.67	90.15	87.62
BESS energy capacity	0.00	100.00	76.56	299.34	297.36	129.86	378.35
PV plant size	0.00	100.00	96.85	99.73	104.98	98.25	104.11
Operational costs (without imports)	100.72	100.00	93.75	93.47	94.08	90.44	88.95
Objective function value	137.17	100.00	96.94	97.08	97.81	95.73	94.88
Imports operational costs	183.10	100.00	98.29	95.70	95.44	96.65	91.97

Table 6 Results for forecasted solar model

Forecasted solar model	0 GT (%)	3a GT (%)	3b EST (%)	3c SIM (%)	4a GT DSM (%)	4b EST DSM (%)	4c SIM DSM (%)
Power contract	104.43	100.00	93.64	92.29	93.67	90.14	87.51
BESS energy capacity	0.00	100.00	76.56	287.83	297.36	145.90	380.90
PV plant size	0.00	100.64	97.38	99.51	105.66	99.20	103.96
Operational costs (without imports)	100.72	99.96	93.72	93.57	94.04	90.40	88.86
Objective function value	137.17	101.11	98.05	97.70	99.00	96.89	95.54
Imports operational costs	183.10	101.63	99.93	96.81	97.19	98.12	93.05

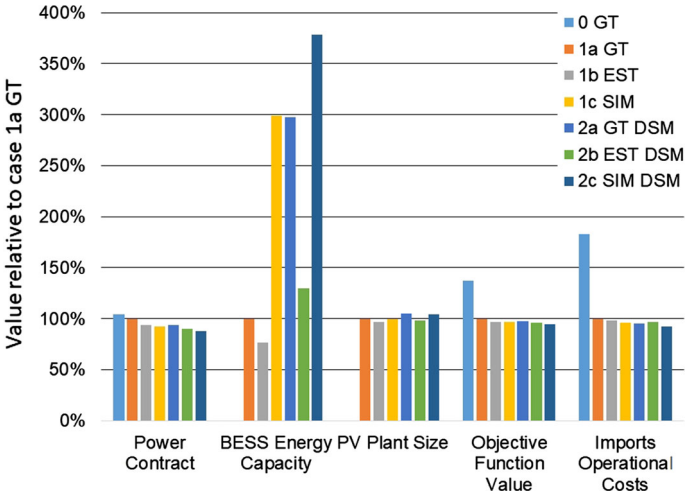

Fig. 9 Optimization results for current solar conditions (cases 0, 1a, 1b, 1c, 2a, 2b, and 2c)

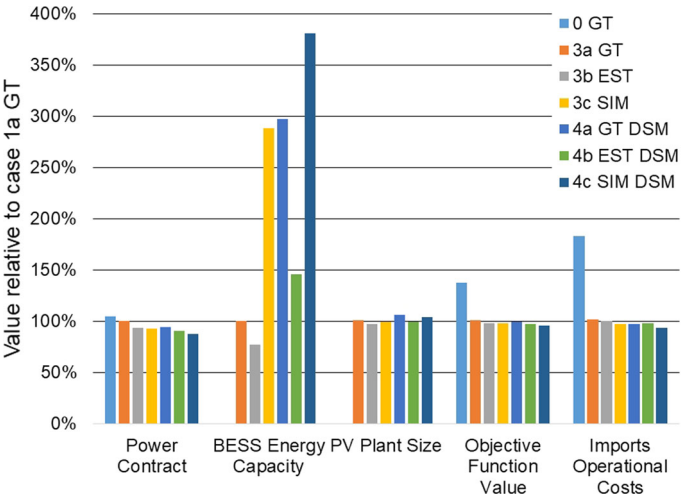

Fig. 10 Optimization results for forecasted solar conditions (cases 3a, 3b, 3c, 4a, 4b, and 4c). Case 0 included for reference

3.2.2 Results Based on Estimated SPI Time Series

The sequence of blocks is fixed and defined by the mine schedule, which depends on the copper grades. Therefore, the sequence of SPI values feeding the SAG mill when stockpiles are not used, or entering the stockpiles when these are considered, is fixed and defined by the block sequence based on grades. Now, decisions are made based on estimated SPI values, which will depart from the optimum decision. The reported objective function in Tables 5 and 6 approximates the actual objective function, and is not actually assessed with the true values, so it should only be considered as a

reference value indicating how well the estimated yearly cost is inferred from the estimated models. The actual objective function, when using the true SPI time series with the sized PV-BESS infrastructure based on the estimated or simulated SPI values, is presented in Table 7. It can be seen that the sizing of the PV-BESS infrastructure using simulated values slightly improves the objective function. This improvement should not be disregarded considering the significant energy cost incurred in mineral processing plants.

Other interesting insights from these results include the fact that, if the variability is underestimated, the size of the PV plant becomes slightly smaller, and the BESS is underestimated, as there is no need for a significantly larger buffer to cover fluctuations in the grindability of the feed to the SAG mill. This can be seen in all cases. The BESS energy capacity using the estimated time series of grindability is sized as only 77% (case 1b) of that of the ground truth (case 1a) without DSM. When DSM is considered, the change in the BESS energy capacity is even more dramatic, going from 297% (case 2a) to 130% (case 2b). This can be explained based on the fact that, when DSM is used, there is more control over the variability of the feed, hence it is safe to invest in a large BESS since it will be used at its full potential. However, if the variability is underestimated due to the smoothing of the SPI estimation, the DSM will not have such a significant effect, and the required battery system will be sized smaller than it should be. Similar trends can be seen in the case with the forecasted solar model.

3.2.3 Results Based on Simulated SPI Time Series

Again, in this case, the objective function reported is evaluated considering the simulated values and not the true values, in Tables 5 and 6, while the actual objective function results are presented in Table 7 (for the current solar conditions). It is interesting to note the effect of the variability on the sizing of the PV and BESS infrastructure. The PV plant tends to be of a size similar to the case of the ground truth. However, the BESS capacity is systematically larger than that defined in the ground truth: 299% (case 1c) versus 100% (case 1a), and 378% (case 2c) versus 297% (case 2a), with similar results being found in the case with the updated solar model. This is balanced by a smaller grid contract and smaller imports operational costs.

Considering the range of possible variations in SPI and solar irradiance simulated for these experiments, the resulting buffer capacity in the battery system becomes very large, to minimize the grid imports beyond the contract, which may prove to be very expensive. The BESS system is thus prepared to buffer a large array of possible combinations of day types.

3.2.4 Results Based on Forecasted Solar Model

The forecasted solar model generates slight increases of 1% in total yearly cost with respect to the current solar model (case 3a versus case 1a or case 4a versus case 2a). As mentioned above, the forecasted solar model implies an increase of the frequency of bad days, along with excellent days, so the effect may not be significant. However, this is a fairly crude forecast model that does not consider the significant change seen

in 2014 onwards. Additional scenarios could be evaluated to investigate the sensitivity of the result when drastic changes are considered.

4 Conclusions

Energy is one of the key resources required to produce raw materials and metals. The mining industry is well aware of the challenges related to the increasing hardness of ores, which translates into higher specific energy consumption, and must search for alternative sources of energy. Solar energy offers a solution to this problem, given the significant development of photovoltaic plants and battery energy storage systems in recent years. In areas where solar power is abundant, integration of this energy source can favorably affect the overall yearly energy cost of a mining operation. This paper presents some of the benefits of the integration of solar energy, in the context of a mineral processing plant, and specifically in relation to the power consumption of a SAG mill.

The effect of the variability of the ore grindability, as well as the variability in solar irradiance to generate the energy in the photovoltaic plant, along with the sizing of a proper battery storage system has been studied. The modeling approach integrates geostatistical simulation of the geometallurgical units in a copper deposit, and cosimulation of the copper grades and the SAG power index, to characterize the joint spatial relationship of the grade and grindability. A sampling campaign over the spatial model is performed to emulate the information available for decision-making in practice. The reserves model is then transferred into a time series by means of a mine plan, and the use of stockpiles is considered, modeling two stocks based on the estimated or simulated SPI values. The specific energy consumption of the rock determines the energy demand of the SAG mill. This energy is supplied by a combination of energy from the grid, which is defined by a power contract, and additional imports that may be required if the contracted demand is exceeded. This energy can be balanced by energy provided by a solar photovoltaic plant along with a battery energy storage system. The energy supplied by this system depends on the solar irradiance at the location where the PV plant is built. A first-order Markov model is built to simulate the variability in day types in terms of solar irradiance, and the hourly energy is mimicked by hot deck imputation from a database of solar irradiance available for the last 13 years. Sizing of the optimum PV-BESS is done using linear stochastic optimization. Finally, the possible change in solar irradiance patterns due to climate change is assessed based on a forecasted model of log ratios of the data types out to the year 2030. Results show that integrating a PV-BESS into a SAG mill generates significant cost reductions and should be studied in all operations where solar availability is high.

Demand-side management (i.e., adapting the demand profile to price signals) can be applied to the SAG mill operation, by creating stockpiles that allow management of the blend or ore fed to the plant. This reduces the overall energy cost of the plant by about 2% in the cases studied. In this case study, it led to larger battery storage, balanced with a smaller grid contract, and smaller imports from the grid when additional energy is needed. This could be further optimized by ensuring a more homogeneous feed, to take full advantage of the PV-BESS infrastructure and ensure optimum use of the

batteries capacity, minimum requirements for overconsumption from the grid, and better grinding performance (not discussed in this paper).

Finally, climate change was considered by forecasting the solar irradiance out to 2030. Although this translates into significant changes in the marginal probabilities of days of different types in relation to the solar irradiance availability, it did not affect the results in a significant manner, leading to a small cost increase. This means that the PV-BESS infrastructure is robust against climate change, needing only a small increase in size to cover future fluctuations in solar patterns. More sophisticated forecasting models could be considered to assess the effect of these changes, as well as a more complex approach to simulate the day types. The current approach uses a first-order Markov chain, which inherently misses weather trends that persist over multiple days.

The presented application integrates modeling approaches from different areas in the mining value chain. It is, in the authors' opinion, a true geometallurgical integration of knowledge from different areas to address a significant challenge in the mining industry, related to its energy intensiveness.

Acknowledgements This work was supported by the Chilean National Commission for Scientific and Technological Research (CONICYT), through the SERC-Chile (CONICYT/FONDAP/15110019) and the Solar Mining Project (CONICYT-BMBF 20140019), and the German Research Foundation through grant DFG-NO 805/11-1. We acknowledge the support of the Natural Sciences and Engineering Research Council of Canada (NSERC) through funding reference nos. RGPIN-2017-04200 and RGPAS-2017-507956.

Appendix

The maximum daily irradiance and the corresponding thresholds to define the day types for each month, based on the 13 years of data available, are presented in Table 7. The corresponding numbers of days of each type are computed in Table 8, and an example transition probability matrix is presented in Table 9.

Table 7 Thresholds for day types for every month

Month	Max. of daily PV	95%	85%	60%
Jan	10.190	9.681	8.662	6.114
Feb	9.395	8.925	7.986	5.637
Mar	8.819	8.378	7.496	5.291
Apr	7.573	7.194	6.437	4.544
May	6.276	5.962	5.335	3.766
Jun	5.477	5.203	4.655	3.286
Jul	6.000	5.700	5.100	3.600
Aug	7.067	6.714	6.007	4.240
Sep	8.483	8.059	7.211	5.090
Oct	9.619	9.138	8.176	5.771
Nov	10.047	9.545	8.540	6.028
Dec	10.378	9.859	8.821	6.227

Table 8 Count of day types per month and additive log ratios

Year	Excellent	Good	Moderate	Bad	Total	ln(E/B)	ln(G/B)	ln(M/B)
2004	47	200	111	8	366	1.771	3.219	2.630
2005	39	210	102	14	365	1.025	2.708	1.986
2006	26	221	113	5	365	1.649	3.789	3.118
2007	46	211	92	16	365	1.056	2.579	1.749
2008	42	234	83	7	366	1.792	3.509	2.473
2009	55	212	90	8	365	1.928	3.277	2.420
2010	46	223	90	6	365	2.037	3.615	2.708
2011	69	184	101	11	365	1.836	2.817	2.217
2012	50	212	98	6	366	2.120	3.565	2.793
2013	44	218	91	12	365	1.299	2.900	2.026
2014	48	197	110	10	365	1.569	2.981	2.398
2015	53	192	99	18	362	1.080	2.367	1.705
2016	68	192	81	24	365	1.041	2.079	1.216

Table 9 Example transition probabilities between day types from solar data (January)

From	To			
	Excellent	Good	Moderate	Bad
Excellent	0.46	0.46	0.08	0.00
Good	0.04	0.69	0.26	0.02
Moderate	0.03	0.56	0.42	0.00
Bad	0.25	0.50	0.25	0.00

References

Armstrong M, Galli AG, Beucher H, Le Loc'h G, Renard D, Doligez B, Eschard R, Geffroy F (2003) Plurigaussian simulations in geosciences, 1st edn. Springer, Berlin

Bouchard J, Desbiens A, Poulin E (2017) Reducing the energy footprint of grinding circuits: the process control paradigm. IFAC-Papers On Line 50(1):1163–1168. https://doi.org/10.1016/j.ifacol.2017.08.402

CEEC (2013) Innovation mining more for less. Report, Coalition for Energy Efficient Comminution. https://www.ceecthefuture.org/resources/innovation-mining-less. Accessed 1 June 2019

Child M, Breyer C, Bogdanov D, Fell HJ (2017) The role of storage technologies for the transition to a 100% renewable energy system in Ukraine. Energy Procedia 135:410–423. https://doi.org/10.1016/j.egypro.2017.09.513

Chiles J-P, Delfiner P (2012) Geostatistics: modeling spatial uncertainty. Wiley series in probability and statistics, 2nd edn. Wiley, New York

Choi Y, Song J (2017) Review of photovoltaic and wind power systems utilized in the mining industry. Renew Sustain Energy Rev 75:1386–1391. https://doi.org/10.1016/j.rser.2016.11.127

Clifton J, Boruff BJ (2010) Assessing the potential for concentrated solar power development in rural Australia. Energy Policy 38(9):5272–5280. https://doi.org/10.1016/j.enpol.2010.05.036

de Bakker J (2014) Energy use of fine grinding in mineral processing. Metall Mater Trans E 1(1):8–19. https://doi.org/10.1007/s40553-013-0001-6

Deutsch CV (2006) A sequential indicator simulation program for categorical variables with point and block data: BlockSIS. Comput Geosci 32:1669–1681

Deutsch JL (2015) Multivariate spatial modeling of metallurgical rock properties, unpublished Ph.D. thesis, University of Alberta

Garrido M, Sepulveda E, Ortiz JM, Navarro F, Townley B (2018) A methodology for the simulation of synthetic geometallurgical block models of porphyry ore bodies. In: Geomet 2018—5th international seminar on geometallurgy, 28–30 Nov 2018, Santiago, Chile

Giurco D, McLellan B, Franks DM, Nansai K, Prior T (2014) Responsible mineral and energy futures: views at the nexus. J Clean Prod 84:322–338. https://doi.org/10.1016/j.jclepro.2014.05.102

Goodfellow R, Dimitrakopoulos R (2017) Simultaneous stochastic optimization of mining complexes and mineral value chains. Math Geosci 49(3):341–360. https://doi.org/10.1007/s11004-017-9680-3

Haas J, Cebulla F, Cao K, Nowak W, Palma-Behnke R, Rahmann C, Mancarella P (2017) Challenges and trends of energy storage expansion planning for flexibility provision in low-carbon power systems—a review. Renew Sustain Energy Rev 80(C):603–619. https://doi.org/10.1016/j.rser.2017.05.201

ICMM (2014) 10 principles, our work, sustainable development framework. International Council on Mining and Metals. http://www.icmm.com/our-work/sustainable-development-framework/10-principles. Accessed 26 Aug 2014

Izenman AJ (2008) Modern multivariate statistical techniques—regression, classification and manifold learning. Springer, New York

Journel AG, Isaaks EH (1984) Conditional indicator simulation: application to a Saskatchewan uranium deposit. Math Geol 16(7):685–718

Lamghari A (2017) Mine planning and oil field development: a survey and research potentials. Math Geosci 49(3):395–437. https://doi.org/10.1007/s11004-017-9676-z

Levesque M, Millar D, Paraszczak J (2014) Energy and mining—the home truths. J Clean Prod 84:233–255. https://doi.org/10.1016/j.jclepro.2013.12.088

Li DHW, Yang L, Lam JC (2012) Impact of climate change on energy use in the built environment in different climate zones—a review. Energy 42:103–112. https://doi.org/10.1016/j.energy.2012.03.044

Manchuk JG, Deutsch CV (2012) A flexible sequential Gaussian simulation program: USGSIM. Comput Geosci 41:208–216. https://doi.org/10.1016/j.cageo.2011.08.013

Mariethoz G, Caers J (2014) Multiple-point geostatistics: stochastic modeling with training images. Wiley, Hoboken

Matthews B, Craig IK (2013) Demand side management of a run-of-mine ore milling circuit. Control Eng Pract 21:759–768. https://doi.org/10.1016/j.conengprac.2013.02.005

Ministerio de Energía de Chile (2018) Explorador Solar. http://www.minenergia.cl/exploradorsolar/. Accessed 15 Nov 2018

Moran CJ, Kunz NC (2014) Sustainability as it pertains to minerals and energy supply and demand: a new interpretative perspective for assessing progress. J Clean Prod 84:16–26. https://doi.org/10.1016/j.jclepro.2014.09.008

Ohunakin OS, Adaramola MS, Oyewola OM, Matthew OJ, Fagbenle RO (2015) The effect of climate change on solar radiation in Nigeria. Sol Energy 116:272–286. https://doi.org/10.1016/j.solener.2015.03.027

Ortega A, Escobar R, Colle S, de Abreu SL (2010) The state of solar energy resource assessment in Chile. Renew Energy 35(11):2514–2524. https://doi.org/10.1016/j.renene.2010.03.022

Ortiz JM, Kracht W, Townley B, Lois P, Cárdenas E, Miranda R, Álvarez M (2015) Workflows in geometallurgical prediction: challenges and outlook. In: Schaeben H, Tolosana-Delgado R, van den Boogaart KG, van den Boogaart R (eds) Proceedings of the 17th annual conference of the International Association for Mathematical Geosciences IAMG 2015

Pamparana G, Kracht W, Haas J, Ortiz JM, Nowak W, Palma-Behnke R (2019a) Studying the integration of solar energy into the operation of a semiautogenous grinding mill. Part I: framework, model development and effect of solar irradiance forecasting. Miner Eng 137:68–77. https://doi.org/10.1016/j.mineng.2019.03.017

Pamparana G, Kracht W, Haas J, Ortiz JM, Nowak W, Palma-Behnke R (2019b) Studying the integration of solar energy into the operation of a semiautogenous grinding mill. Part II: effect of ore hardness variability, geometallurgical modeling and demand side management. Miner Eng 137:53–67. https://doi.org/10.1016/j.mineng.2019.03.016

Paraszczak J, Fytas K (2012) Renewable energy sources – a promising opportunity for remote mine sites? In: International conference on renewable energies and power quality (ICREPQ'12), 28–30 Mar 2012

Pelzer R, Mathews EH, le Roux DF, Kleingeld M (2008) A new approach to ensure successful implementation of sustainable demand side management (DSM) in South African mines. Energy 33(8):1254–1263. https://doi.org/10.1016/j.energy.2008.03.004

Perez C, Ortiz JM (2011) Mine-scale modeling of lithologies with multiple-point geostatistical simulation. In: Mathematical geosciences at the crossroads of theory and practice, IAMG 2011, Salzburg, 5–9 Sept 2011

Schaeffer R, Szklo AS, Frossard A, Lucena AFP, Borba BSMC, Nogueira LPP, Fleming FP, Troccoli A, Harrison M, Boulahyad MS (2012) Energy sector vulnerability to climate change: a review. Energy 38(1):1–12. https://doi.org/10.1016/j.energy.2011.11.056

Starkey J, Dobby G (1996) Application of the Minnovex SAG Power Index Test at five Canadian SAG plants. In: Proceedings autogenous and semiautogenous grinding, pp 345–360

Tolosana-Delgado R, Mueller U, van den Boogaart KG (2018) Teaching aid: geostatistics for compositional data: an overview. Math Geosci. https://doi.org/10.1007/s11004-018-9769-3

Wei D, Craig IK (2009) Grinding mill circuits—a survey of control and economic concerns. Int J Miner Process 90(1–4):56–66. https://doi.org/10.1016/j.minpro.2008.10.009

Zweibel K, Mason K, Fthenakis V (2007) A solar grand plan. Sci Am 298(1):64–73. https://doi.org/10.1038/scientificamerican0108-64